Deciphering background fractures from damage fractures in fault zones and their effect on reservoir properties in microporous carbonates (Urgonian limestones, SE France)

Irène Aubert, J. Lamarche, Philippe Leonide

Deciphering background fractures from damage fractures in fault zones and their effect on reservoir properties in microporous carbonates (Urgonian limestones, SE France)

I. Aubert*, J. Lamarche & P. Léonide
Aix-Marseille Universite, Marseille, France
*E-mail: aubert@cerege.fr

Abstract
Most carbonates have a dual porosity and permeability (matrix and fracture). As fractures are preferential conduits for fluid flows, fracture networks strongly impact reservoir hydraulic properties. Two fracture patterns can affect reservoirs: random background fractures in the host rock and damage zone clustered fractures in fault zones. This study identifies the structural and diagenetic attributes of both fracture patterns and determined their respective impact on reservoir properties. The study focuses on the East part of La Fare Anticlinal (SE France). Lower Cretaceous, Urgonian facies carbonates underwent a polyphase tectonic history. Faults were set up as normal and were later reactivated as strike-slip. We made a 290m scan-line along the outcrop to characterize fracture network in and outside the fault zones. The diagenetic analysis on 45 thin sections in Polarized Light Microscopy, with SEM and cathodoluminescence evidenced 3 cementation phases and 2 micrite recrystallization phases. This study shows that fault zone structural properties and deformation are dependent of initial host rock background fractures network. Fault zone structure with damage zone fracture network encouraged the fluid to flow and the cementation of S2 phase. This fluid flow, absent in the host rock strongly modified the reservoir properties of the studied zone.

Natural fracture networks impact the underground reservoir properties especially in carbonates (Philip et al. 2005; Gale et al. 2010; Lamarche et al. 2012; Lavenu et al. 2013). Carbonates represent ~60% of the world hydrocarbon reservoirs. Therefore, characterizing and understanding the genesis of fracture networks and their impact on permeability is a major challenge for hydrocarbon exploration and production. The majority of fractures affecting reservoirs can be considered as background fractures randomly distributed throughout the rock mass (Vitale et al. 2012; Lavenu et al. 2013). Unlike background fractures, fault related fractures are discontinuously distributed in the host rock but are clustered along fault zones. Faults are 3D complex zones classically divided into three structural domains: the undeformed protolith (so-called 'host-rock' in the present paper), the damage zone and the fault core, along which most of the displacement is accommodated (Chester & Logan 1986, 1987; Caine et al. 1996; Hammond & Evans 2003). Depending on the fault architecture and diagenetic history, fault zones can be conduits (Evans et al. 1997; Reches & Dewers 2005; Agosta et al. 2007, 2008, 2012; Molli et al. 2010; Delle Piane et al. 2016; Huisman 2016; Sinisi et al. 2016), seals (Tondi 2007; Agosta et al. 2010) or mixed zones (Matonti et al. 2012). In most fault zones, the fracture network in the damage zone form an effective fluid pathway and constitutes the structural unit with the highest permeability (Evans et al. 1997; Reches & Dewers 2005; Agosta et al. 2007, 2008, 2012; Molli et al. 2010; Delle Piane et al. 2016; Sinisi et al. 2016). Background fractures in the host rock either form effective fluid pathways or barriers (Larsen et al. 2010; Lamarche et al.

2012). Indeed, structural and diagenetic properties of fractures are the result of poly-phase tectonics (e.g. burial, tectonic stresses) and mechanical evolution. In carbonates, the latter strongly depends on facies, diagenesis and pre-existing fracture network (Laubach et al. 2009; Lamarche et al. 2012; Lavenu et al. 2014; Lavenu & Lamarche 2018). The poly-phase evolution induces multiple modifications of the fluid flow pathways and thus the strong alteration of reservoir properties, enhanced by carbonates sensitivity to diagenetic processes. In fact, carbonate petrological and petrophysical properties tend to change easily over time (Lambert et al. 2006; Fournier & Borgomano 2009; Deville de Periere et al. 2017) and this sensitivity is coupled with fractures occurrence (Billi et al. 2003; Carpentier et al. 2015). Fractures are an important factor in the modifications of carbonate diagenetic properties and have a strong impact on reservoir properties (Laubach et al. 2018). Hence, it is important to characterize fracture-induced diagenetic events, with coupled structural and diagenetic approaches in order to determine the reservoir properties evolution trough time. The aim of this study is to (1) identify the influence of pre-existing background fractures on fault zones formation and (2) determine the impact of background and fault-related fractures on reservoir petrophysical properties by defining their respective structural and diagenetic attributes. We conducted a high resolution structural survey of an outcrop in order to discriminate the respective properties of fault zone versus background fractures. To determine the diagenetic impact of fractures on carbonate reservoir properties, we performed a detailed petrophysical and petrological analysis coupled with isotopic measurements.

I. Geological context

The studied faults are located in South-East Basin (SE France) and affect Barremian, Urgonian facies carbonates. The present-day basin architecture results from a long-lasting succession of tectonic events affecting the basin development. During Jurassic and lower cretaceous, the opening of the Tethys Ocean led to carbonate platform deposition (Dercourt 2000; Léonide *et al.* 2007). During Late Hauterivian–Early Aptian time-interval, the Urgonian platform of Provence developed (Léonide *et al.* 2014). Subsequently, during the Albian, a regional uplift so-called "Durancian uplift" led to E-W faults (Masse & Philip 1976; Guyonnet-Benaize et al. 2010) and to erosion of Early Barremian rocks, inducing an important stratigraphic hiatus of about 39My. The return to platform deposit conditions during late Cretaceous led to of transgressive rudist platforms (Philip 1970). Thereafter, still during late cretaceous (from ≈80My to ≈40My ; Molliex (2009); Bestani (2015)) the basin located in the foreland of Pyreneo-Provençal orogeny, underwent a tectonic inversion. The N-S shortening gave rise to E-W to NE-SW-trending thrust faults and ramp folds (Guieu 1967; Tempier 1987; Guyonnet-Benaize et al. 2010; Molliex et al. 2011; Lavenu et al. 2013) and transpressional reactivation of the earlier faults (Champion et al. 2000). During Oligo-Miocene times, the tectonic context turned to extension as the area was located in the Ligurian back-arc basin (Lacombe & Jolivet 2005). Lastly, the far field Alpine NW-SE to N-S stress dimly reactivated Pyreneo-Provençal structures (Champion et al. 2000; Guyonnet-Benaize et al. 2010) from Miocene-Pliocene (≈14My; Champagnac *et al.* (2004); Delacou *et al.* (2004); Cushing *et al.* (2008)).

The studied outcrop is located on the southern limb of the E-W-trending La Fare Anticline (Roche 2008; Fig. 1) affected by an E-W and NE-SW-trending fault network (Roche 2008; Matonti et al. 2012). Faults affect the upper Hauterivian, the lower Barremian and the Santonian units dipping 25°S (Fig. 1A). Upper Hauterivian unit is composed of marly external plateform carbonates topped by decametric marly limestones bearing chert (Masse 1976). The Lower Barremian unit (Urgonian facies) is composed of infra- to supra-littoral platform carbonates made of thin to coarse bioclastic calcarenites (Roche 2008). The lower Barremian is truncated by the Durancian erosion surface and is uncomfortably covered by Santonian coarse rudist limestones (Fig 1.B). A highway road-cut across the fold exhibits a fresh Barremian calcarenite section where we observe background fractures interfering with a complex fault zone including five polyphase faults (Fig. 1.C).

II. Methods

The goal of this study is to identify the influence of pre-existing background fractures on fault zones formation and to determine the impact of background fractures and fault-related fractures on reservoir properties through time. To this purpose we conducted structural and petrophysical analyses of faults and fractures in carbonates and a stratigraphic log after Dunham classification (Dunham 1962). In this study, the term "fracture" refers to mode I discontinuities (opening mode, (Aydin 2000; Gudmundsson 2004), including joints and veins.

A. Field data

We performed a SSE-NNW, 250 meters long 1-D scanline sampling nine parameters on each single fracture: strike, dip, type (joint, stylolithes, vein, fault), graduation, spacing with fracture of the same set, visible height, aperture, fill (calcite, barren, oxydes), cross-cutting relationship between fractures. SSE-NNW outcrop orientation can induce a bias on fracture measurement. Along the outcrop, within fault zones and host rock we measured 1650 of fractures, veins and styloliths. Stereographic projections and rose diagrams have been realized in order to sort fractures by strike. After sorting, we calculated fracture type proportions within 2m windows along scanlines, continuously in the fault zone and every 5 meters in the host rock. To image fractures in the fault zone, fractures have been drawn on pictures to emphasize the architecture and structural characteristics of each single fault and of the whole fault zone.

B. Laboratory analyses

We collected 44 samples to measure porosity and analyze the diagenetic sequence on thin-sections. 30 of the samples were systematically collected every 2 meters along section. In addition, we collected 14 samples in peculiarly interesting places around faults. 44 samples were re-plugged (2.54×2.54cm cylindric dry plugs) in the laboratory and in order to performed porosity measurements with a Micromeritics AccuPyc 1330 helium pycnometer. The pycnometer measured macroporosity (>30µm) and microporosity (<10 µm) after the equation:

$$\phi = ((Vb - Vg)/Vb) \times 100$$

Where ϕ is the porosity in percent, Vg is the matrix volume of the plug and Vb is the bulk volume of the sample. The sample bulk volume was determined by immersion of the sample in a known volume of water.

The characterization of microfacies of rock samples has been performed on 45 thin sections impregnated with a blue-epoxy resin to highlight the porosity. Thin sections were observed with the cathodoluminescence technics using a Technosyn Cold Cathode Luminescence Model 8200 Mk II coupled to an Olympus_ BH2 microscope and to a Zeiss_ MRc5. It highlighted the diagenetic phases (cement, dissolution, recrystallization…). Stable carbon and oxygen isotopes ($\delta^{13}C$ and $\delta^{18}O$) were measured to determine the paleo-fluid nature. To this purpose, 59 microsamples were micro-drilled from polished thin sections with an 80 µm diameter microsampler (Merkantec Micromill) at the VU University (Amsterdam, Netherlands). Carbon and oxygen values were obtained with the Gasbench II and the Finnigan DeltaPlus IRMS. Values are reported in PDB (Vienna PEE Dee Belemnite). Reproducibility was ±0.02 for carbon isotopes and ±0.05% for oxygen isotopes. Characterization of major element compositions and morphologies of micrite crystals were determined on thin sections and on freshly broken surfaces with Scanning electron microscopy (SEM) using PHILIPS XL30 ESEM with a current set at 20kV at Aix-Marseille University (France).

III. Structural analysis of fault zone and background fractures

The outcrop is a 250m-long vertical road-cut with an average bedding striking N045° and dipping 25° to the south. The outcrop includes: (*i*) a 50m-long fault zone comprising 5 polyphase sub-vertical faults (F1 to F5 from south to north), (*ii*) a 200m-long un-faulted zone, so-called 'host rock' in this paper, bearing background fractures (Fig. 2A, 2B). All fractures affecting both zones are bed-perpendicular. They are sorted into 5 sets (Fig. 2 C, 2D): two major sets trending N030° and N120° and 3 minor sets trending N000°, N060° and N090°. On the outcrop, we do not observe cross-cutting relationships allowing to decipher the timing for fracture chronology.

A. Fault zone architecture

Faults are NNE-SSW- to NE-SW-trending (Fig. 2A& 2D). The details of their attitude are given in table 1. Fault displacement is not discernible due to the monotony of the sedimentary units (calcarenites).We have measured 870 fractures in the damage zones comprising 863 joints and 7 veins. Veins are located close to F2 and F3, were karstic filling is also observed (Fig. 2A). Fractures are distributed in the five sets as follows: 14% of N000°, 33.5% of N030°, 11% of N060°, 10.5% of N090° and 31% of N120°. Fracture heights range from 30cm to 500cm with an average of 51.5cm (SD: 61cm), with 82% of fractures smaller than 80cm (Fig. 2D). .

In the fault cores we discriminate two fault rocks (Fig. 2B): fault rock A (FRA) is composed of a cohesive breccia with rounded clasts from the damage zone and a white cemented matrix. It is linked to first activation of faults. Fault rock B (FRB) results from the faults reactivation. It is composed of angular to sub-angular clasts of FRA, of clasts of the damage zone surrounding FRA and of a non-cemented orange/oxided matrix (<20%). Clasts of FRA are included in FRB.

The 5 faults are bordered by asymmetrical damage zones which are described, from south to north, as follows (Fig. 2A, 2B):

F1- The southern damage zone of F1 is made of an 18m-wide low fractured damage zone (fracture density 6.1m^{-1}). Fractures are parallel to the fault plane. The N060° and N090° fracture sets are absent in the first two meters, then largely occur (N090°: 19.5% and N060°: 20.5%). The F1 fault core is 20cm-width and bear FRA. North of F1, a 7m-long damage zone with a fracture density of 7.7m^{-1} is made of fractures conjugate to the fault plane, including 23.4% of N000°, 40% of N030°, 23.5% of N060°, 11% of N120° and only 1.5% of N090°.

F2- The southern damage zone of F2 is 6m-wide. It is sparsely fractured with a high fracture density of 11.7 m^{-1} composed mostly of N060° and N090° sets (respectively 27.5% and 20.1%). An increase of these two sets is noticed 2m on side of the F2 fault plane. F2 fault core is 10 to 15 cm-thick and is formed by FRB. Centimetric to metric paleo-karst occur along beds and joints (Fig. 2A, 2B).

F3- The northern damage zone of F2 is the southern damage zone of F3. The F3 core thickness varies between 0 and 15cm and is made of FRB. North to F3 a 2m-wide dimly fractured damaged zone comprises 50% of N060°, 33.3% of N030° and 16.7% of N000°.

F4- The damage zone South of F4 is highly fractured (15.3m^{-1}) along 8m. It is made of conjugated-to- and parallel-to-fault fractures. The southern part of F4 is peculiar because it contains very few N060° and N090° fractures, respectively 4% and 2.4%. The core of F4 is 20cm-wide, made of FRA and FRB. Fractures are parallel to F4 in the 4m aside from the fault plane. The damage zone between F4 and F5 is characterized by a "close to breccia" fracture pattern of N060° and N090°.

F5- The F5 fault core is composed of FRB with a thickness ranging from 50cm to 1m. North of it, the 2m-wide damage zone is sparsely fractured by N030° (27.7%) and N120° (61%) fracture sets.

Except between F4 and F5, the stratigraphic bedding is still visible in all damage zones.

B. Background fracture pattern

From the north of fault F5 we can consider that we measured background fractures in the host rock. The so-called host rock is marked by a consequent increase of N120° (40%) and N030° (45%) fractures and a reduction of N000° (8.5%), NN060° (4.5%) and N090° (2%) ones (Fig. 2C, 2D). Background fractures in the host rock are not filled by any cement. The fracture height is 80cm in average (SD 99cm). Some fractures of the N000° set are highly persistent (> 6m, Fig. 2Da). The average fracture density is 7.43m^{-1} in average, reaching 11.71 m^{-1} between 110 and 115m on the measured scan-line.

Fault zone and host rock present close fracture density values (average of respectively 9.45m-1 and 7.43m-1). Hence, differentiating both zones with this criterion is tricky. However, the

N090° set mainly occur close to fault planes. Hundred meters apart from F5 the N090° frequency is <2%, while it is >10% close to the fault. Inferred from this, we place the fault zone boundary 15m apart from F5, where the N090° set frequency is <2%.

IV. Petrophysical and diagenetic evolution

The matrix porosity decreases from > 16% in the host rock to an average of 3.5% in the fault zone. The lowest values are systematically observed in 2 meters-wide zones south of each single fault, as well as between F4 and F5 (Fig. 3A, 3B). The high values are observed north of F1, F3 and F5. Hence, the porosity decrease is asymmetrical and disharmonic in the fault zone. The porosity analysis with blue-epoxy resin on 45 thin-sections highlights the porous rock-type (ϕ > 15%) in the host rock affected by background fractures and the tight rock-type (ϕ < 5%) near the faults (Fig. 3C). The porous rock-type enclose two types of porosity: a micro-porosity in the micrite and a macro-porosity in moldic pores linked to micritic dissolution. In the tight facies the reduced porosity is mostly located in barren styloliths (Fig. 3C).

The porosity evolution in both background fractures and fault zone has been compared with the diagenetic evidence on thin sections. Three cementation phases (S0, S1 and S2) and 2 types of micrite microfabrics (MF1 and MF3 *sensu* Fournier et al. 2014 and Léonide at al., 2014) have been identified (Fig. 3D). Both fault zones and host rock are affected by S0 and S1. The first cement S0 is a non-luminescent isopachous cement growing with equal thickness (≈10µm) around all micritized grains during the early diagenesis. The second cement S1 can be divided in 2 sub-phases: S1a in intergranular spaces composed of a sparitic non-luminescent calcite and S1b with a bright luminescence covering S1a and filling micro-porosity in micritized grains (Fig. 3D). Both cements occur in the entire outcrop, are not specific to the fault zone and do not filled fractures. The cement S1 (eq. to C1 in Aubert et al. 2018) is related to the Durancian uplift.

The S2 cement is a blocky calcite occurring in veins, in matrix of FRA and in intergranular and moldic pores of fault zone (Fig. 3D). It is absent in the host rock. This cement exhibits zones of non-luminescent and bright luminescent bands. It can be divided into two sub-phases: S2a is non-luminescent with some highly luminescent band, and S2b is bright luminescent with some non-luminescent bands. Isotopic values of S2 show a mix between the two sub-zones S2a and S2b and range from -4.09 to +0.39‰ for $\delta^{13}C$ and from -8.09 to -4.77‰ for $\delta^{18}O$. The FRA matrix has isotopic values ranging from –7.1 to -6.7 ‰ for $\delta^{18}O$ and from -4.0 to -1.1 ‰ for $\delta^{13}C$ (Fig. 3E). As S2 is present in FRA matrix as well as in fault zone veins, we deduce that it is synchronous to first fault activity during the Pyrenean shortening.

A micritisation phase (M1) affected all grains (bioclasts, ooids and peloids) during the early diagenesis (Purser 1980; Samankassou et al. 2005; Vincent et al. 2007; Léonide et al. 2014). This phase can be linked to micro-bores organisms at the sediment-water interface. Within the micritised grain, we observed two micrite micro-fabrics with SEM according to Fournier *et al.* (2011) taking into account the crystals shape and contacts. In the host rock, the micrite is loosely packed and coalescent with puntic subrounded, anhedral /subhedral crystals (MF3,

Fig. 3F). Within the fault zone, the micrite is tight with compact subhedral mosaic crystals (MF1,Fig. 3G). The fault zone micro-fabric MF1 has low porosity values of < 5% while the MF3 micro-fabric in host rock is associated to porosity values >15%.

Isotopic measurements conducted on bulk rock gave values ranging from -8.1 to -5.2‰ for $\delta^{18}O$ and -3.4 to +1.1‰ for $\delta^{13}C$ (Fig. 3E). Most values plot outside the "Barremian sea water calcite box" which ranges from +1.00 to +3.00‰ for $\delta^{13}C$ and from -1.00 to -4.00‰ for $\delta^{18}O$ (Moss & Tucker 1995; Godet et al. 2006). This indicates that bulk rock values have been strongly impacted by secondary diagenetic processes. The measurements in the host rock have less negative $\delta^{13}C$ isotopic values (mean of -5.9‰ for $\delta^{18}O$ and -0.97‰ for $\delta^{13}C$) than the rock within fault zone (mean of -6.7‰ for $\delta^{18}O$ and -1.7‰ for $\delta^{13}C$). In addition to the diagenetic modifications, we also observed the occurrence of karsts near F2, particularly south of it. These karsts have sedimentary, laminar infill composed of micrite, calcite clast and oxides. The karstic infill has isotopic values like S2 of -7.43‰ for $\delta^{18}O$ and -2.23‰ for $\delta^{13}C$ (Fig. 3E)

V. Discussion

The description of macro- and micro-structures associated to faults compared to the host rock background fractures, as well as the isotopic results on host rocks and fractures described above, allows to discuss the inheritance of background fractures when faults formed, and their respective consequences on reservoir properties of carbonates for million years with respect to the geodynamic history of the basin.

A. Structural evolution

All faults observed in the fault zones and the host rocks have specific relationships and geometry that can be interpreted in terms of relative timing and geodynamics. The N030° and N120° fracture sets occur along the entire outcrop with a constant frequency. Their relative frequency does not increase in the fault zone. As they show no sensitivity to the fault zone, it means that they predate the fault zone formation. Concerning the geodynamic conditions of their setting, two hypotheses are to be considered:

(1) Lamarche et al. (2012) have reported the occurrence of these two sets apart from faults over a regional area and around the study outcrop. These authors linked their occurrence to an early burial loading, giving rise to two perpendicular, bed-normal fracture sets.

(2) these fractures cross-cut the cement S1 which formed during the early stage of the regional Durancian uplift (Aubert et al. 2018). They formed prior to faults which originated during Pyrenean shortening. Implicitly, the fractures might be linked to a late stage of the Mid-Cretaceous Durancian uplift (Fig.4A).

The faults striking N030° (F1, F2 & F5) are parallel to early N030° fractures. We can deduce that these faults were reactivated fractures of this set. As the F3 and F4 are not parallel to N030° or N120° fracture sets they are considered as neo-formed.

The N090° and N060° fracture sets occur mainly in the fault zones (average frequency of respectively 11% and 12%) and less within host rock (average frequency of respectively 4.5% and 2%). They can be linked to the N030° faults activity which is attributed to the Pyrenean shortening (Aubert et al. 2018). The N000° set occurs along the entire outcrop, but its frequency is higher in the fault zone (14%, Fig. 2Db) than in the host rock (8, 5%, Fig. 2Dc). This set strikes parallel to the Pyrenean maximum horizontal stress direction oriented N000° to N170° (Guieu 1967; Tempier 1987; Le Pichon et al. 1988; Champion et al. 2000; Ford et al. 2006; Pichon et al. 2010; Molliex et al. 2011; Espurt et al. 2012). Thus, it can be associated to the event leading to the fold setting and bedding & faults tilting of 25° towards the South.

The fault rocks present within fault core are markers of faults activities. Using inclusion principles is it possible to determine that FRA pre-date PRB. Hence, FRA is associated to first fault activity and FRB to the second.

B. Inheritance of background fractures on fault zone development

What was the impact of the background fracture network on fault formation during Pyrenean shortening? After Mohr-Coulomb theory, the compressive paleo-stress conditions linked to the Pyrenean event in Provence is favorable for reactivating the N030° fractures as sinistral faults, and the N120° fractures in a dextral kinematics. Consequently, the studied faults striking N030° are due to the strike-slip reactivation of these pre-existing fractures (Fig. 4B). There is evidence for neither N030° nor N120° fracture reactivation elsewhere within the outcrop. The localized reactivation of N030° fractures as faults inhibits further strain accommodation elsewhere in the host rock. Despite the strain localization, the bulk fracture density in the damage zone is only slightly higher (mean of 9.45m-1) than in the host rock (mean of 7.43 m^{-1}). The N060°- and N090°-striking fracture sets related to fault activity constitute only 11% and 10.5%, respectively, of fractures in the fault zone. This relatively small fracture increase can have four origins:

(i) The maximum damage zone along faults may be only localized at their tip (Cowie & Scholz 1992; Vermilye & Scholz 1999; d'Alessio & Martel 2004; Kim et al. 2004). Consequently, it is possible that the road-cut has intersected faults in their central part, where the fault planes localized the deformation, explaining the reduced fracture density in the damage zone.

(ii) *Filbrandt et al.* (2007) have shown that faults may have little damage zones close to their initiation point while throwing. Indeed, once the failure is initiated in the rock, no damage occurs any more but only slip. The pre-existing fractures would have formed failure zones favoring slipping without damage rather than fracturing.

(iii) The five faults are part of a larger fault zone. The faults would, consequently, form sub-faults sharing the strain. The amount of strain accommodation distributed on each sub-fault may be sufficient, what explains why damage zones are reduced.

(iv) In damage zones of normal faults, fractures have strikes mechanically linked to the main fault (Caine et al. 2010). In the studied fault zone where the major faults striking

N030°, reactivation of N030° fractures would have been privileged compared to N060° and N090° fracture sets.

In addition, the F3, N058°-striking and 80°-dipping, has even lower fracture density in its damage zone. As F4, this fault makes an angle of ~60° with the Pyrenean σ_H. This is not fully compatible to be neo-formed faults, and poorly favorable to be reactivated faults. Considering their strikes, these faults do not reactivate N030° joints like the other faults. These faults exhibit no kinematic indicators. Moreover, F3 has a reduced and discontinuous fault core with a maximum thickness of 15cm and thinly fractured damage zone. Therefore, F3 and F4 can be rejoining faults between F2 and F5.

C. Fault zones versus background fractures diagenesis, impact on reservoir properties

The rocks exposed in the studied outcrop recorded two main diagenetic events which did not similarly affect the host rock and the fault zone. Therefore, specific diagenetic events were responsible for the rock-type differentiation, leading to a porous host rock and a tight fault zone (fig. 4). These events are:

(1) the cementation phase S1 filling intergranular space and the micrite re-crystallization (MF3; Ostwald ripening processes; Ostwald 1886; Volery et al. 2010a, b) leading to the development of microporosity during the Durancian uplift (Fig. 4A, Léonide et al. 2014),

(2) The cementation phase S2 post-dating the faults setting. The S2 fluids flew through the faults and the damage zone, leading to the cementation of veins, fault core and karstification processes. Indeed, as described in the chapter "Petrophysical and diagenetic evolution", the karstic infill has isotopic values (-7.43‰ for $\delta^{18}O$ and -2.23‰ for $\delta^{13}C$) similar to S2 values (from -4.09 to +0.39‰ for $\delta^{13}C$ and from -8.09 to -4.77‰ for $\delta^{18}O$). This similarity indicates that the karstic sediments were carried by fluids similar to those of S2 cement.

Fault zone bulk values (mean of -6.7‰ for $\delta^{18}O$ and -1.7‰ for $\delta^{13}C$) are close to the cement S2 isotopic values. This reveals that the bulk rock in fault zones have been largely saturated by the fluids which gave rise to S2 cement. Considering that the bulk isotopic values are impacted by micrite isotopy, the measured bulk values can be explained by micrite cementation with S2. This micrite cementation led to a strong decrease of porosity in the fault zone. Isotopic values of S2 (from -4.09 to +0.39‰ for $\delta^{13}C$ and from -8.09 to -4.77‰ for $\delta^{18}O$) highlight a strong influence of meteoric fluid during cementation process (Dickson & Coleman 1980; Allan & Matthews 1982; Swart 2015)being responsible for the clogging of fault zone porosity. The S2 cement is not observed in the host rock. This lack can be either due to:

(i) the absence of S2 fluid flow in the host rock, or
(ii) the occurrence of S2 fluid flow but no cementation, or
(iii) the occurrence of S2 fluid flow and cementation with later complete dissolution.

Fluid flow in carbonates can lead to cementation and/or dissolution. Significant flows are necessary to dissolve pre-existing cements. When important dissolution occur, dissolution features can be observed such as vuggs cross-cutting cementation phases for example (Flügel 2004). Since none of these features are noticed in the studied host rock, the hypothesis (iii)

cannot be considered. If the fracture network in the host rock was the path for fluids to flow, the S2 cement would be observed in the host rock bearing background fractures. The fluids giving rise to S2 are characterized by negative $\delta^{13}C$ values. The host rock $\delta^{13}C$ values are higher (ranging from -1.3‰ to -0.6‰ with a mean of -1.2‰) than fault zone bulk values (ranging from -3.4‰ to -1.4‰ with a mean of -2.1‰). As the $\delta^{13}C$ values of the host rock are less negative than in the fault rock, it indicates that S2 fluid flow did not impact the host rock isotopic characteristics. The host rock bulk isotopic values are close to values measured in another part of La Fare Anticlinal: In the Castellas Fault zone, bulk $\delta^{13}C$ values range from -1.4‰ to 0.5‰ with a mean of -0.6‰. This corresponds to values measured in C1 which is linked to a fluid flow dated of the Mid-Cretaceous Durancian uplift (Aubert et al. 2018). Consequently, the isotopic values and the lack of S2 cementation in the host rock show that the host rock has not been impacted by S2 fluid flow. This invalidates the (ii) hypothesis and confirms the hypothesis (*i*) which is absence of S2 fluid flow in the host rock. Thus, this fluids only flew through the fault zone. This interpretation is surprising considering the fracture arrangement. In the host rock, fracture N000°- and N030°-trending are metric and dense (average density of $7.43m^{-1}$). They cross-cut each other with an angle of 30°, leading to a well-connected fracture network (Fig. 4A). Besides, fractures have to be favorably oriented to the regional constraint to be opened (Sibson 2000; Agosta et al. 2010; Caine et al. 2010). In the studied outcrop, fractures were favorably oriented regarding the regional Pyrenean σ_H to be open. Nevertheless, no S2 fluid flow occurred in the host rock. Hence, all fluids flew through the fault zone. It could be due to structural and permeability properties of the fault zone. In the study area, faults have decametric to kilometric dimension with a large drainage area that induces a fault parallel flow (Matonti et al. 2012). The dense fracture network of the damage zone of faults enhance and favor fluid circulations in fault damage zones (Caine et al. 1996; Sibson 2000; Walker et al. 2013; Rotevatn & Bastesen 2014; Dimmen et al. 2017; Peacock et al. 2017). In the case of the studied fault zone, the S2 cements -and therefore the fluid flow- is essentially localized very close to the fault planes (maximum 10m-wide), meaning that the damage zone is less permeable than the fault core (Fig.4B). This differs from most faults in carbonates, where the damage zone is the preferential fluid pathway, whereas the fault core is a low-permeability wall (Evans et al. 1997; Reches & Dewers 2005; Agosta et al. 2007, 2008, 2012; Molli et al. 2010; Delle Piane et al. 2016; Sinisi et al. 2016). Why is it different in fault zones in carbonates of Provence? There, the fault cores are thin and not cemented. They are composed of breccia with enhanced permeability. This fault core style has been described in strike-slip and extensional faults affecting carbonate formations of Apennines (Italy) by *Billi et al.* (2003) and *Storti et al.* (2003). As a result, fault cores formed an across- and along-fault effective fluid pathway (Billi et al. 2008; Delle Piane et al. 2016). Hence, the fault zone with decametric to kilometric slip surfaces associated with high permeability breccia and a well-connected fracture network drained fluids with a meteoric component.

D. Reservoir property evolution with time: towards a conceptual model

The structural and diagenetic evolution with time is different in the fault zone and in the host rock. It led to reservoir compartmentalization and to the evolution of the reservoir from type IV to type I (classes after Nelson 2001; Fig. 5) as follows:

(1) During Barremian times andearly burial, the Urgonian carbonates reservoir properties were due to the high porosity and permeability of the matrix, corresponding to a type IV reservoir. Background fractures formed as orthogonal sets during early (~20Ma) and shallow (~300-400m) burial and changed the reservoir from type IV to type III (Nelson 2001).

(2) The Durancian uplift led to the micro-porosity development through micrite recrystallization MF3 within grains. Microporous limestones are known to have high matrix porosity and low to moderate matrix permeability (Jack & Sun 2003; Deville de Periere et al. 2011). In the case of the studied micro-porous Urgonian carbonates, the permeability is essentially localized in the well-connected barren fracture network which forms efficient flow pathways. Therefore, these rocks formed a type III reservoir with matrix porosity and fracture permeability (Nelson 2001).

(3) The Pyrenean shortening led to well-connected, dense, non-cemented fractures in the fault zones and to a breccia in the fault core (FRA). The fracture network in faults formed an efficient fluid pathway, where fluids flew parallel to the fault plane. This drainage is increased by the high permeability of the fault core (FRA), inducing an intense fluid circulation during the early stages of fault activity. It led to micrite cementation (MF1) and to a strong porosity decrease in the matrix (Fig. 5B). This modified initial reservoir properties in the fault zone vicinity from type III to type I. The localized flow responsible for S2 cementation did not affect the surrounding host rock what preserved the type III properties of host rock apart from faults. (Nelson 2001) (Fig. 5C).

(4) During final alpine exhumation, the reservoir properties of the host rock evolved with a porosity increase link to micrite dissolution (Fig. 5B).

VI. Conclusion

In the present paper, we deciphered the structural and fluid interactions between host rock, background fractures and fault zones in carbonates during the basin evolution lasting for 130 Ma.

- We unraveled two pre-fault, burial-induced perpendicular fracture sets (N030° and N120°) and three fault-related fracture sets (N000°, N060° and N090°), with their relative proportions and intensity.
- Quantitative analysis of fracture sets along the scan line crossing the fault zone is an efficient tool to differentiate early fractures from fault-induced fractures within the fault zone.
- F1, F2 and F5 result from the slip-reactivation of the N030° background fractures, consequently, the fault zone structure is inherited from pre-existing background fractures and the dim development of the N060° and N090° fracture sets related to faults in the damage zone. This structure can be explained by the concentration of strain on pre-existing N030° background fractures; on secondary fault planes of a larger fault zone) and/or to the preferential development of N030° fractures.

- Differential fluid flows along fault planes led to the cementation of micro-porosity, fractures and intergranular porosity and thus to a strong decrease of the fault zone porosity. Cementation phases modified initial reservoir properties in the fault zone vicinity from type III to type I.
- Background fractures and fault relative fractures impacted differently the carbonate reservoir properties and led to reservoir compartmentalization.

Our results emphasize that fault zone development & architecture depend on pre-existing fracture networks and that diagenesis in fault zone strongly impact the carbonates reservoir properties and modify the reservoir behavior vis-à-vis fluid flow. This multiple approach combining structural, diagenetic and geochemical analyses is appropriate for a full understanding of faulted and fractured carbonate reservoirs through time in underground reservoirs.

Acknowledgements

The authors gratefully acknowledge Pascal Richard and Rolland Salardon (Aix-Marseille University) for their useful discussions on respectively structural and diagenetic aspects. The author greatly thank APIC Cerege whose financial support allowed isotopic measurements. Thanks to Lionel Marié (Aix-Marseille University) for making the studied thin sections.

Agosta, F., Prasad, M. & Aydin, A. 2007. Physical properties of carbonate fault rocks, Fucino Basin (Central Italy): implications for fault seal in platform carbonates. *Geofluids*, **7**, 19–32.

Agosta, F., Mulch, A., Chamberlain, P. & Aydin, A. 2008. Geochemical traces of CO2-rich fluid flow along normal faults in central Italy. *Geophysical Journal International*, **174**, 1074–1096.

Agosta, F., Alessandroni, M., Antonellini, M., Tondi, E. & Giorgioni, M. 2010. From fractures to flow: A field-based quantitative analysis of an outcropping carbonate reservoir. *Tectonophysics*, **490**, 197–213.

Agosta, F., Ruano, P., Rustichelli, A., Tondi, E., Galindo-Zaldívar, J. & Sanz de Galdeano, C. 2012. Inner structure and deformation mechanisms of normal faults in conglomerates and carbonate grainstones (Granada Basin, Betic Cordillera, Spain): Inferences on fault permeability. *Journal of Structural Geology*, **45**, 4–20.

Allan, J.R. & Matthews, R.K. 1982. Isotope signatures associated with early meteoric diagenesis. *Sedimentology*, **29**, 797–817.

Allmendinger, R.W., Cardozo, N. & Fisher, D.M. 2013. Structural geology algorithms: Vectors and tensors. *Cambridge University Press*, **9781107012**, 1–289.

Aubert, I., Lamarche, J., Léonide, P. & Salardon, R. 2018. Fault zones diagenesis through time: impact on drain properties. Case study in Urgonian carbonates of La Fare massif (Provence – SE France). *In*: *RST - 26th Earth Science Meeting*. 122.

Aydin, A. 2000. Fractures, faults, and hydrocarbon entrapment, migration and flow. *Marine and Petroleum Geology*, **17**, 797–814.

Bestani, L. 2015. *Géométrie et Cinématique de l'avant-Pays Provençal : Modélisation Par Coupes Équilibrées Dans Une Zone à Tectonique Polyphasée.* Aix-Marseille University.

Billi, A., Salvini, F. & Storti, F. 2003. The damage zone-fault core transition in carbonate rocks: Implications for fault growth, structure and permeability. *Journal of Structural Geology*, **25**, 1779–1794.

Billi, A., Primavera, P., Soligo, M. & Tuccimei, P. 2008. Minimal mass transfer across dolomitic granular fault cores. *Geochemistry, Geophysics, Geosystems*, **9**.

Caine, J.S., Evans, J.P. & Forster, C.B. 1996. Fault zone architechture and permeability structure. *Geology*, **24**, 1025–1028.

Caine, J.S., Bruhn, R.L. & Forster, C.B. 2010. Internal structure, fault rocks, and inferences regarding deformation, fluid flow, and mineralization in the seismogenic Stillwater normal fault, Dixie Valley, Nevada. *Journal of Structural Geology*, **32**, 1576–1589.

Cardozo, N. & Allmendinger, N.W. 2013. Sperical projections with OSXStereonets. *Computers & Geosciences*, **51**, 193–205.

Carpentier, C., Ferry, S., Lecuyer, C., Strasser, A., Geraud, Y. & Trouiller, A. 2015. Origin of Micropores In Late Jurassic (Oxfordian) Micrites of the Eastern Paris Basin, France. *Journal of Sedimentary Research*, **85**, 660–682.

Champagnac, J.D., Sue, C., Delacou, B. & Burkhard, M. 2004. Brittle deformation in the inner NW Alps: From early orogen-parallel extrusion to late orogen-perpendicular collapse. *Terra Nova*, **16**, 232–242.

Champion, C., Choukroune, P. & Clauzon, G. 2000. La déformation post-miocène en provence occidentale. *Geodinamica Acta*, **13**, 67–85.

Chester, F.M. & Logan, J.M. 1986. Implications for Mechanical Properties of Brittle Faults from Observations of the Punchbowl Fault Zone, California. *PAGEOPH*, **124**.

Chester, F.M. & Logan, J.M. 1987. Composite planar fabric of gouge from the Punchbowl Fault, California. *Journal of Structural Geology*, **9**.

Cowie, P.A. & Scholz, C.H. 1992. Physical explanation for the displacement-length relationship of faults using a post-yield fracture mechanics model. *Journal of Structural Geology*, **14**, 1133–1148.

Cushing, E.M., Bellier, O., et al. 2008. A multidisciplinary study of a slow-slipping fault for seismic hazard assessment: The example of the Middle Durance Fault (SE France). *Geophysical Journal International*, **172**, 1163–1178.

d'Alessio, M.A. & Martel, S.J. 2004. Fault terminations and barriers to fault growth. *Journal of Structural Geology*, **26**, 1885–1896.

Delacou, B., Sue, C., Champagnac, J.D. & Burkhard, M. 2004. Present-day geodynamics in the bend of the western and central Alps as constrained by earthquake analysis. *Geophysical Journal International*, **158**, 753–774.

Delle Piane, C., Giwelli, A., et al. 2016. Frictional and hydraulic behaviour of carbonate fault gouge during fault reactivation — An experimental study. *Tectonophysics*, **690**, 21–34.

Dercourt, J., Gaetani, M., et al. 2000. Peri-Tethys Atlas: Palaeogeographical Maps. *Paris, Commission for the Geological Map of the World*, 24.

Deville de Periere, M., Durlet, C., Vennin, E., Lambert, L., Bourillot, R., Caline, B. & Poli, E. 2011. Morphometry of micrite particles in cretaceous microporous limestones of the middle east: Influence on reservoir properties. *Marine and Petroleum Geology*, **28**, 1727–1750.

Deville de Periere, M., Durlet, C., Vennin, E., Caline, B., Boichard, R. & Meyer, A. 2017. Influence of a major exposure surface on the development of microporous micritic limestones - Example of the Upper Mishrif Formation (Cenomanian) of the Middle East. *Sedimentary Geology*, **353**, 96–113.

Dickson, J.A.D. & Coleman, M.L. 1980. Changes in carbon and oxygen isotope composition during limestone diagenesis. *Sedimentology*, **27**, 107–118.

Dimmen, V., Rotevatn, A., Peacock, D.C.P., Nixon, C.W. & Nærland, K. 2017. Quantifying structural controls on fluid flow: Insights from carbonate-hosted fault damage zones on

the Maltese Islands. *Journal of Structural Geology*, **101**, 43–57.

Dunham, R.J. 1962. Classification of Carbonate Rocks According to Depositional Textures. *Classification of Carbonate Rocks--A Symposium*, **1**, 108–121.

Espurt, N., Hippolyte, J.C., Saillard, M. & Bellier, O. 2012. Geometry and kinematic evolution of a long-living foreland structure inferred from field data and cross section balancing, the Sainte-Victoire System, Provence, France. *Tectonics*, **31**.

Evans, J.P., Forster, C.B. & Goddard, J. V. 1997. Permeability of fault-related rocks, and implications for hydraulic structure of fault zones. *Journal of Structural Geology*, **19**, 1393–1404.

Filbrandt, J.B., Richard, P.D. & Franssen, R. 2007. Fault growth and coalescence: Insights from numerical modelling and sandbox experiments. *GeoArabia*, **12**, 17–32.

Flügel, E. 2004. Microfacies of Carbonate Rocks Analysis, Interpretation and Application. 996.

Ford, M., Duchene, S., Gasquet, D. & Vanderhaeghe, O. 2006. Two-phase orogenic convergence in the external and internal SW Alps. *Journal of the Geological Society*, **163**, 815–826.

Fournier, F. & Borgomano, J. 2009. Critical porosity and elastic properties of microporous mixed carbonate-siliciclastic rocks. *Geophysics*, **74**, E93–E109.

Fournier, F., Leonide, P., Biscarrat, K., Gallois, A., Borgomano, J. & Foubert, A. 2011. Elastic properties of microporous cemented grainstones. *Geophysics*, **76**, E211–E226.

Gale, J.F.W., Lander, R.H., Reed, R.M. & Laubach, S.E. 2010. Modeling fracture porosity evolution in dolostone. *Journal of Structural Geology*, **32**, 1201–1211.

Godet, A., Bodin, S., et al. 2006. Evolution of the marine stable carbon-isotope record during the early Cretaceous: A focus on the late Hauterivian and Barremian in the Tethyan realm. *Earth and Planetary Science Letters*, **242**, 254–271.

Gudmundsson, A. 2004. Effects of Young's modulus on fault displacement. *Comptes Rendus - Geoscience*, **336**, 85–92.

Guieu, G. 1967. Un exemple de tectonique tangentielle: l'évolution du cadre montagneux de Marseille. *Bulletin de la Société Géologique de France*, **7 (T.IX N°**, 610–630.

Guyonnet-Benaize, C., Lamarche, J., Masse, J.P., Villeneuve, M. & Viseur, S. 2010. 3D structural modelling of small-deformations in poly-phase faults pattern. Application to the Mid-Cretaceous Durance uplift, Provence (SE France). *Journal of Geodynamics*, **50**, 81–93.

Hammond, K.J. & Evans, J.P. 2003. Geochemistry , mineralization , structure , and permeability of a normal- fault zone , Casino mine , Alligator Ridge district , north central Nevada. **25**, 717–736.

Huisman, J.G.S. and B.A.H. 2016. Toward the creation of models to predict static and dynamic fault-seal potential in carbonates.

Jack, A. & Sun, S. 2003. Controls on Recovery Factor in Fractured Reservoirs: Lessons Learned from 100 Fractured Fields. *Proceedings of SPE Annual Technical Conference and Exhibition*.

Kim, Y.S., Peacock, D.C.P. & Sanderson, D.J. 2004. Fault damage zones. *Journal of Structural Geology*, **26**, 503–517.

Lacombe, O. & Jolivet, L. 2005. Structural and kinematic relationships between Corsica and the Pyrenees-Provence domain at the time of the Pyrenean orogeny. *Tectonics*, **24**, 1–20.

Lamarche, J., Lavenu, A.P.C., Gauthier, B.D.M., Guglielmi, Y. & Jayet, O. 2012. Relationships between fracture patterns, geodynamics and mechanical stratigraphy in Carbonates (South-East Basin, France). *Tectonophysics*, **581**, 231–245.

Lambert, L., Durlet, C., Loreau, J.P. & Marnier, G. 2006. Burial dissolution of micrite in Middle East carbonate reservoirs (Jurassic-Cretaceous): Keys for recognition and timing. *Marine and Petroleum Geology*, **23**, 79–92.

Larsen, B., Grunnaleite, I. & Gudmundsson, A. 2010. How fracture systems affect permeability development in shallow-water carbonate rocks: An example from the Gargano Peninsula, Italy. *Journal of Structural Geology*, **32**, 1212–1230.

Laubach, S.E., Olson, J.E. & Gross, M.R. 2009. Mechanical and fracture stratigraphy.

Laubach, S.E., Lamarche, J., Gauthier, B.D.M., Dunne, W.M. & Sanderson, D.J. 2018. Spatial arrangement of faults and opening-mode fractures. *Journal of Structural Geology*, **108**, 2–15.

Lavenu, A.P.C. & Lamarche, J. 2018. What controls diffuse fractures in platform carbonates ? Insights from Provence (France) and Apulia (Italy). *Journal of Structural*

Geology, **108**, 94–107.

Lavenu, A.P.C., Lamarche, J., Gallois, A. & Gauthier, B.D.M. 2013. Tectonic versus diagenetic origin of fractures in a naturally fractured carbonate reservoir analog [Nerthe anticline, Southeastern France. *AAPG Bulletin*, **97**, 2207–2232.

Lavenu, A.P.C., Lamarche, J., Salardon, R., Gallois, A., Marié, L. & Gauthier, B.D.M. 2014. Relating background fractures to diagenesis and rock physical properties in a platform-slope transect. Example of the Maiella Mountain (central Italy). *Marine and Petroleum Geology*, **51**, 2–19.

Le Pichon, X., Bergerat, F. & Roulet, M.-J. 1988. Plate kinematics and tectonics leading to the Alpine belt formation; A new analysis. *Geological Society of America*, **218**, 111–131.

Léonide, P., Floquet, M. & Villier, L. 2007. Interaction of tectonics, eustasy, climate and carbonate production on the sedimentary evolution of an early/middle Jurassic extensional basin (Southern Provence Sub-basin, SE France). *Basin Research*, **19**, 125–152.

Léonide, P., Fournier, F., et al. 2014. Diagenetic patterns and pore space distribution along a platform to outer-shelf transect (Urgonian limestone, Barremian-Aptian, SE France). *Sedimentary Geology*, **306**, 1–23.

Masse, J.-P. & Philip, J. 1976. Paléogéographie et tectonique du Crétacé moyen en Provence: révision du concept d'isthme durancien. *Revue de Géographie physique et de Géologie dynamique*, **18**, 49–46.

Masse, J.P. 1976. *Les Calcaires Urgoniens de Provence (Valanginien-Aptien Inférieur) - Stratigraphie, Paléontologie, Paléoenvironnements et Leur Évolution.* Marseille, Thèse de la Faculté des Sciences de Luminy (U2).

Matonti, C., Lamarche, J., Guglielmi, Y. & Marié, L. 2012. Structural and petrophysical characterization of mixed conduit/seal fault zones in carbonates: Example from the Castellas fault (SE France). *Journal of Structural Geology*, **39**, 103–121.

Molli, G., Cortecci, G., et al. 2010. Fault zone structure and fluid–rock interaction of a high angle normal fault in Carrara marble (NW Tuscany, Italy) // Fault zone structure and fluid–rock interaction of a high angle normal fault in Carrara marble (NW Tuscany, Italy). *Journal of Structural Geology*, **32**, 1334–1348.

Molliex, S. 2009. Caractérisation de la déformation tectonique récente en Provence (Sud-Est France). *Centre Européen de Recherche et d'Enseignement en Géosciences de*

l'Environnement, **Thèse de D**, 346.

Molliex, S., Bellier, O., Terrier, M., Lamarche, J., Martelet, G. & Espurt, N. 2011. Tectonic and sedimentary inheritance on the structural framework of Provence (SE France): Importance of the Salon-Cavaillon fault. *Tectonophysics*, **501**, 1–16.

Moss, S. & Tucker, M.E. 1995. Diagenesis of Barremian-Aptian platform carbonates (the Urgonian Limestone Formation of SE France): near-surface and shallow-burial diagenesis. *Sedimentology*, **42**, 853–874.

Nelson, R. 2001. *Geologic Analysis of Naturally Fractured Reservoirs*, second ed.

Ostwald, W. 1886. Lehrbuch der allgemeinen Chemie. *Verlag von Wilhelm Engelmann, Leipzig*, **2**, 909.

Peacock, D.C.P., Dimmen, V., Rotevatn, A. & Sanderson, D.J. 2017. A broader classification of damage zones. *Journal of Structural Geology*, **102**, 179–192.

Philip, J. 1970. *Les Formations Calcaires à Rudistes Du Crétacé Supérieur Provençal et Rhodanien. Thèse de Doctorat, Université de Provence (Marseille).*

Philip, Z.G., Jr, J.W.J., Olson, J.E. & Laubach, S.E. 2005. Modeling Coupled Fracture-Matrix Fluid Flow in Geomechanically Simulated Fracture Networks.

Pichon, X. Le, Rangin, C., Hamon, Y., Loget, N., Lin, J.Y., Andreani, L. & Flotte, N. 2010. Geodynamics of the france southeast basin. *Bulletin de la Societe Geologique de France*, **181**, 477–501.

Purser, B.H. 1980. Sédimentation et diagenèse des carbonates néritiques récents, Les éléments de la sédimentation et de la diagenèse. *Editions Technip*, **1**, 366.

Reches, Z. & Dewers, T.A. 2005. Gouge formation by dynamic pulverization during earthquake rupture. *Earth and Planetary Science Letters*, **235**, 361–374.

Roche, V. 2008. Analyse structurale et géo-mécanique de réseau de failles du chaînon de La Fare les Oliviers (Provence). *Université de Montpellier 2*, 45.

Rotevatn, A. & Bastesen, E. 2014. Fault linkage and damage zone architecture in tight carbonate rocks in the Suez Rift (Egypt): implications for permeability structure along segmented normal faults. *Geological Society, London, Special Publications*, **374**, 79–95.

Samankassou, E., Tresch, J. & Strasser, A. 2005. Origin of peloids in Early Cretaceous deposits, Dorset, South England. *Facies*, **51**, 264–273.

Sibson, R.H. 2000. Fluid involvement in normal faulting. *Journal of Geodynamics*, **29**, 469–499.

Sinisi, R., Petrullo, A.V., Agosta, F., Paternoster, M., Belviso, C. & Grassa, F. 2016. Contrasting fault fluids along high-angle faults: a case study from Southern Apennines (Italy). *Tectonophysics*, **690**, 206–218.

Storti, F., Billi, A. & Salvini, F. 2003. Particle size distributions in natural carbonate fault rocks: Insights for non-self-similar cataclasis. *Earth and Planetary Science Letters*, **206**, 173–186.

Swart, P.K. 2015. The geochemistry of carbonate diagenesis: The past, present and future. *Sedimentology*, **62**, 1233–1304.

Tempier, C. 1987. Modèle nouveau de mise en place des structures provençales. *Bulletin de la Societe Geologique de France*, **3**, 533–540.

Tondi, E. 2007. Nucleation, development and petrophysical properties of faults in carbonate grainstones: Evidence from the San Vito Lo Capo peninsula (Sicily, Italy). *Journal of Structural Geology*, **29**, 614–628.

Vermilye, J.M. & Scholz, C.H. 1999. Fault propagation and segmentation: Insight from the microstructural examination of a small fault. *Journal of Structural Geology*, **21**, 1623–1636.

Vincent, B., Emmanuel, L., Houel, P. & Loreau, J.P. 2007. Geodynamic control on carbonate diagenesis: Petrographic and isotopic investigation of the Upper Jurassic formations of the Paris Basin (France). *Sedimentary Geology*, **197**, 267–289.

Vitale, S., Dati, F., Mazzoli, S., Ciarcia, S., Guerriero, V. & Iannace, A. 2012. Modes and timing of fracture network development in poly-deformed carbonate reservoir analogues, Mt. Chianello, southern Italy. *Journal of Structural Geology*, **37**, 223–235.

Volery, C., Davaud, E., Foubert, A. & Caline, B. 2010a. Lacustrine microporous micrites of the Madrid Basin (Late Miocene, Spain) as analogues for shallow-marine carbonates of the Mishrif reservoir formation (Cenomanian to Early Turonian, Middle East). *Facies*, **56**, 385–397.

Volery, C., Davaud, E., Durlet, C., Clavel, B., Charollais, J. & Caline, B. 2010b.

Microporous and tight limestones in the Urgonian Formation (late Hauterivian to early Aptian) of the French Jura Mountains: Focus on the factors controlling the formation of microporous facies. *Sedimentary Geology*, **230**, 21–34.

Walker, R.J., Holdsworth, R.E., Armitage, P.J. & Faulkner, D.R. 2013. Fault zone permeability structure evolution in basalts. *Geology*, **41**, 59–62.

Figure Captions

Figure 1: Geological context of the study area. A: Simplified structural map with the location of the studied road cut; B. Stratigraphic column of exposed cretaceous carbonates in La Fare anticline (left, modified from Roche 2008) and along the studied cliff (right). C. Picture of a part of the outcrop including the five faults F1 to F5.

Figure 2: A: Fracture mapping in the fault zone (left) and host-rock (right) and, localization of the faults F1 to F5; B: pictures of the outcrop of fault rocks (a), of F2 & F3 (b), of F4 & F5 (c) and of host rock (d, e) A; C. Normalized fracture frequency sorted after fracture strike along the scan-line. Values are calculated continuously within 2m bins in the fault zone and every 10m in the host-rock; D. from left to right: fracture height histogram, stereographic projections of poles to fractures (density contoured), bedding (dashed lines) and faults (red points) using OSXStereonet 10.2.8 (Allmendinger et al. 2013; Cardozo & Allmendinger 2013) and fracture strike pie chart of the fault zones and of the host rock with background fractures.

Figure 3: A: overview picture of the fault zone. B: porosity values measured across the fault zone; C: Pictures of the pore types in fault zone (a & b) and in the host rock (c); D. Pictures of thin section cathodoluminescence showing S0 , S1 & S2 cement and the MF1 micrite ; E. Isotopic analysis of δ13C and δ18O) measured on bulk rock, cement phases, and on micrite. Range values of “Urgonian marine box” have been determined from Moss & Tucker (1995) and Godet et al. (2006); F: MEB pictures of microporosity (white arrow) linked to MF3 micrite micro-frabric; G: MEB picture of the tight MF1micrite micro-fabric.

Figure 4: Schematic evolution of multi-scale reservoir properties through time in the fault zone and the host rock.

Figure 5: Conceptual evolution of the reservoir properties of the study area through 130 My. A: Subsidence/uplift curve of Barremian basement (modified after Lamarche et al. 2012) and main tectonic and diagenetic events from 1 to 4. B: relative porosity evolution of the host rock and fault zone. C. Evolution of the reservoir types after Nelson 2001 during stages 1 to 4.

Table 1: different faults characteristics

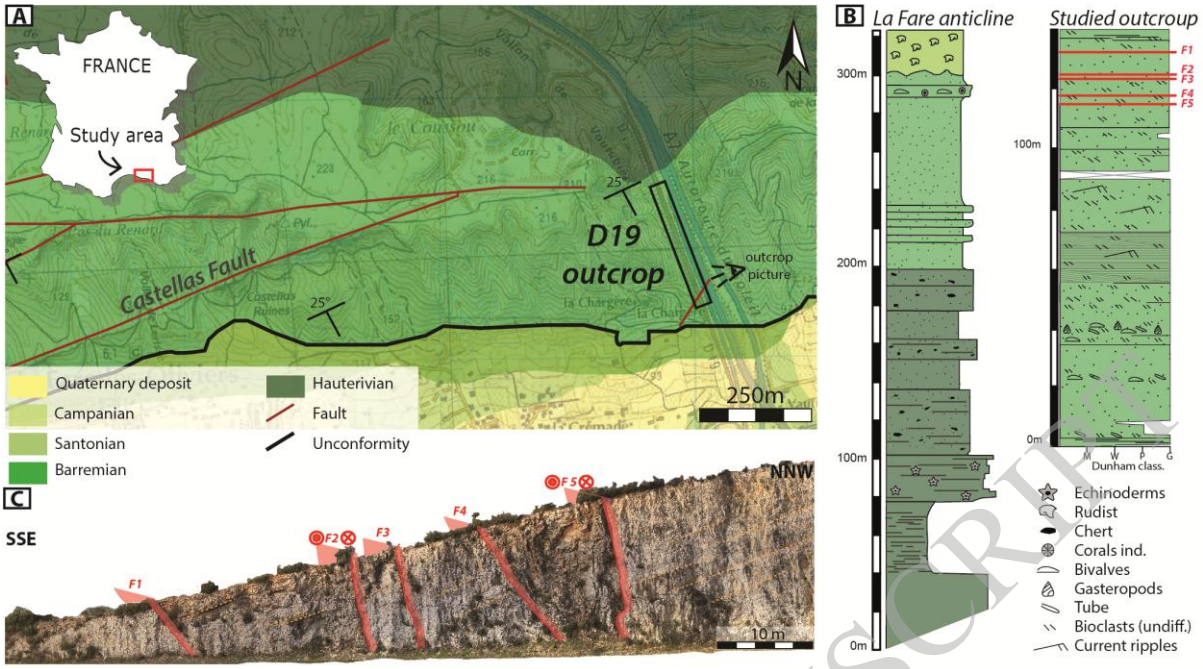

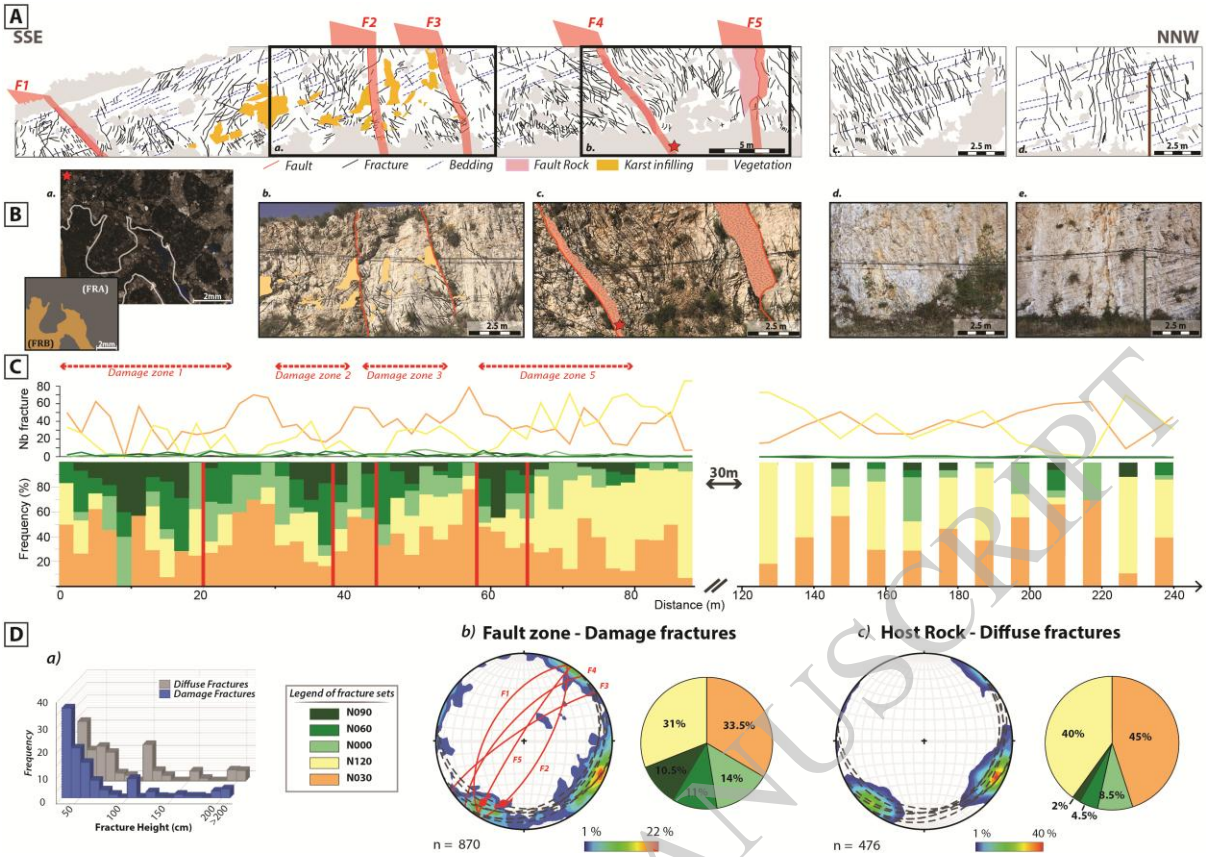

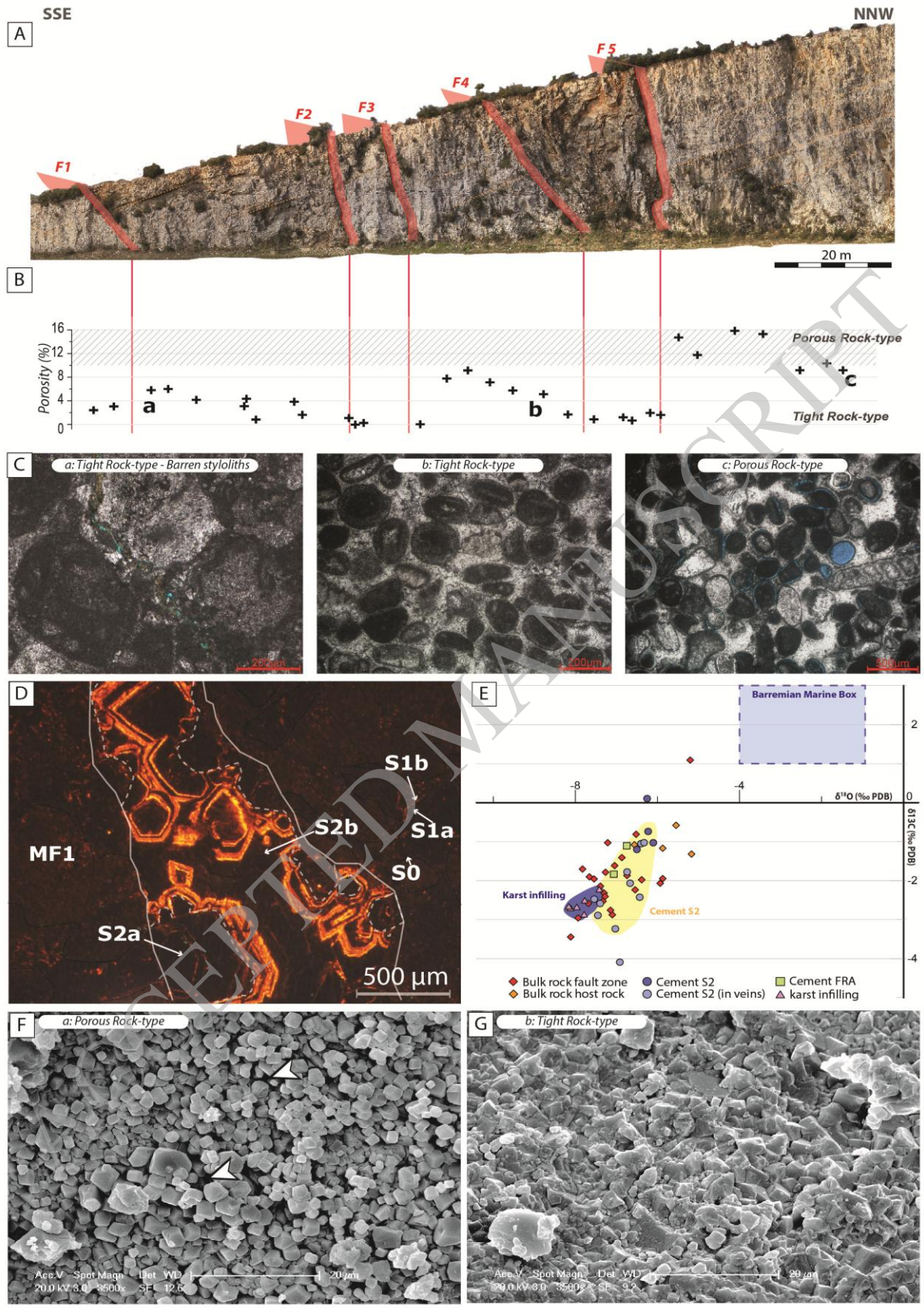

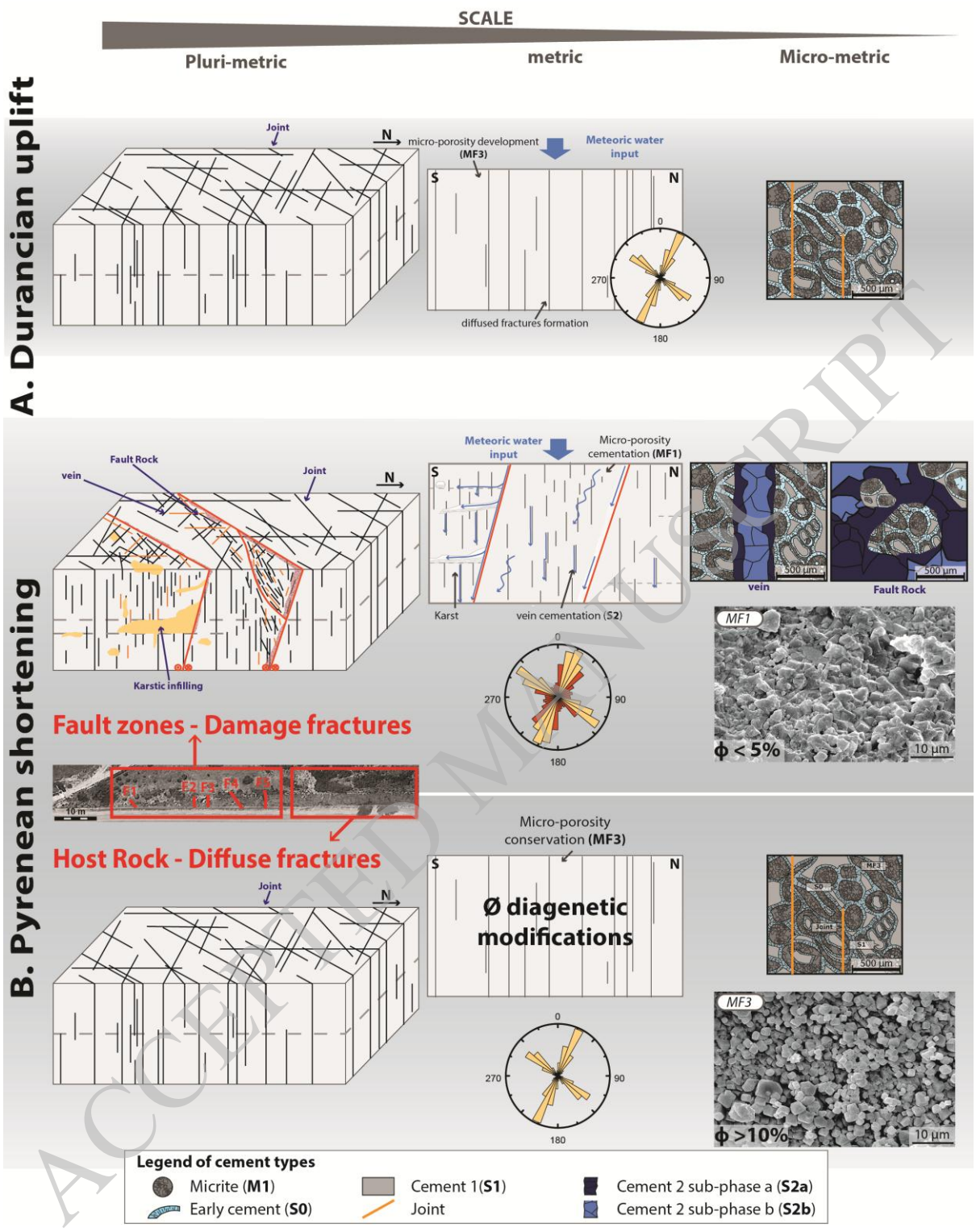

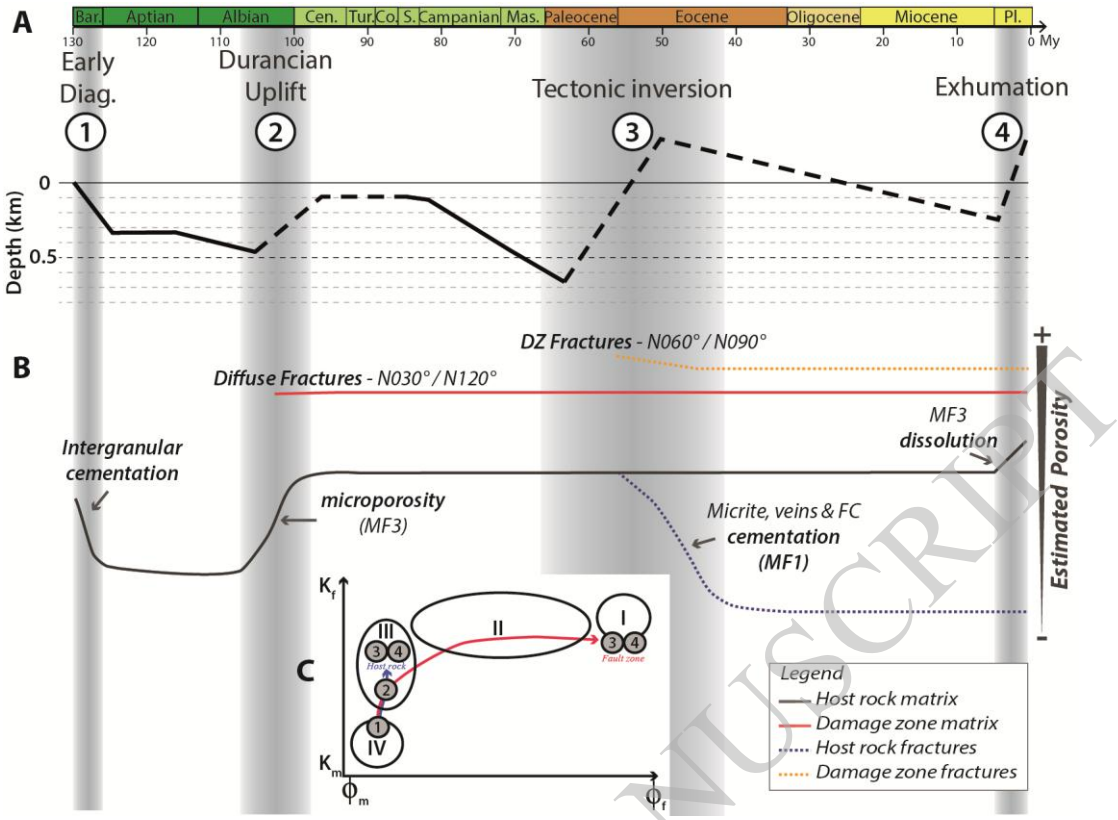

Faille	Direction	Dip	Dip direction	pitch striation	Fault core thickness	Breccia characteristics		
						Fault rock type	Clast	
							Clast morphology	clast size
F1	030	56	W		20	FRA	Sub-angular to subrounded	<10 cm
F2	029	70	E	28 S	10 to 15	FRA ? / FRB	Sub-angular to subrounded	<10 cm
F3	056	80	N		0 to 15	ND	ND	ND
F4	042	70	W		20	FRA / FRB	FRA : Rounded FRB : Angular	< 5 cm < 10 cm
F5	032	85	N	20 SW	50 to100	FRB	Sub-angular to sub-rounded	< 50cm